

Impacts of Land Cover Changes on Rainfall-Runoff and Sediment Transport Processes in The Kelani River, Sri Lanka

Dissanayaka Mudiyanseage Pavithra Sudeshika^{*1}, Yoshiyuki Imamura², Daisuke Harada³ and Shinji Egashira⁴

^{1,2}Department of Civil and Environmental Engineering, Tokyo Metropolitan University, Japan. Email:

¹<pavithrasudeshi@gmail.com>, ²<imamura@tmu.ac.jp>

^{3,4}International Centre for Water Hazards and Risk Management (ICHARM), Public Water Research Institute (PWRI), Japan. Email: ³<harada@icharm.org>; ⁴<egashirasn@mail2.acsnet.ne.jp>

*Corresponding author: D. M. P. Sudeshika, Email: <pavithrasudeshi@gmail.com>

Received: December 3, 2024; Accepted: June 12, 2025; Published: June 20, 2025

ABSTRACT

The present study examines the impacts of land use change on rainfall-runoff, and sediment transportation together with occurrences of landslides in the Kelani River Basin, using MODIS Global yearly land cover data, a physically based distributed rainfall-sediment-runoff model, and a sediment erodibility/ landslide index model. It was realized that the predominant land-use types within the basin were identified as woody savannas, forest, cropland, and built-up areas, and the forest area decreased by 15% and 8.3% of the total basin in 2010 and 2022, respectively, compared to 2001. These alterations in land use correspond to changes in the peak flow discharge and sediment transport rates. This study highlights that the sediment hydrograph changes more sensitively compared to the changes in the flood hydrograph caused by land cover alterations, as the bedload rate is proportional to flow discharge raised to the power of 3/2.

Keywords: MODIS land cover, rainfall-sediment-runoff model, Sediment transport rates, flood flow

1. INTRODUCTION

The Kelani River is significant in Sri Lanka, flowing through Colombo, Capital of the Sri Lanka. It ranks third in terms of water resources in the country and provides hydropower at its upstream location, as well as supplying 90% of Colombo's drinking water, and industrial sand for an extended period, while also supporting a substantial biodiversity ecosystem. However, anthropogenic activities, primarily urbanization and sand mining in the basin, have resulted in

riverbed lowering, riverbank erosion, salt intrusion up to the Ambatale water treatment plant, deterioration of water quality and biodiversity, and flooding in the downstream area (CRIP, 2018). In the current situation of the river system, it is socially imperative to restore river sustainability. Sediment transport processes in the river system are crucial in the river ecosystem which influences river morphology, water quality, habitat formation, nutrient cycling and disturbance regimes. Therefore, it is important to examine the sediment transport processes at the

basin scale to solve these issues and restore river sustainability.

Land use has a considerable impact on surface runoff, sediment transport, and soil erosion (Güvel, 2024). The alteration and mismanagement of land for various purposes have led to changes in the rainfall-runoff characteristics of the basin, which impact the hydrological and sediment regimes of the basin. It is crucial to consider the effects of land-use changes on hydrological and sediment transport processes, which can provide valuable information for the development of water resource management and land-use planning strategies (Zuo et al., 2016). One of the significant alterations in land cover change can be considered as urbanization which is influenced by increased speed and magnitude of the runoff with a dramatic increase of imperviousness in the forms of roofs, roads, and parking lots and reduced infiltration as well as reduced the rainfall storage with vegetation removal (Choi and Deal, 2008; Ohana-Levi et al., 2015). The study by Areu-Rangel et al. (2024) highlights that a 35% reduction in forest areas caused to increase in erosion and sediment transport in mountainous regions in the Yaqui River Basin, Mexico using satellite imagery and Iber software (Version 2.5.2). The increase in Forest has led to a decrease in suspended sediment in the Çakıt sub-basin, Türkiye using Coordination of Information on the Environment (CORINE) land use cover data and sediment observation data (Güvel, 2024).

Conventional methods for evaluating soil erosion, and sediment transport include field measurements and empirical models such as the Universal Soil Loss Equations (USLE), and its modifications (RUSLE). Numerous studies have

been conducted to investigate the impacts of land use changes on rainfall-runoff (Daramola et al., 2022; dos Santos et al., 2020; Choto and Fetene, 2019), sediment yield, and soil erosion (Sourn et al., 2022; Moisa et al., 2021). However, many of these studies have primarily employed simple statistical models or lack physical processes of watersheds. The rainfall-sediment-runoff model is a distributed, physically based model, allowing it to consider the temporal and spatial sediment grain size distribution to determine sediment transport rates. In contrast, most sediment models consider a single median grain-size class of sediment, even though bed-material sediment grain size information is critical for understanding riverine sediment processes (Abeshu et al., 2022).

The objective of this research is to evaluate the effects of land use change on rainfall-runoff, and sediment transport processes at the basin scale using numerical simulations, GIS, and remote sensing data. This study utilized the rainfall-sediment-runoff model to simulate sediment transport processes in the Kelani River basin, considering land use changes from 2001 to 2022. We utilized the MODIS Land Cover Type product (MCD12Q1) with a spatial resolution of 500 m for this purpose. MCD12Q1 is a widely used global land use data product in remote sensing, and it is updated annually, making it highly significant for Earth surface research. One of the main features of this data is spatial and temporal class harmonization, making it an ideal input for hydrological modeling across various regions of the world (Chirachawala et al., 2020). First, this study analyses land cover changes from 2001 to 2022 using the MODIS Land Cover Type product (MCD12Q1). Then, this study evaluates the flood

hydrographs, hydrographs of bedload rates, suspended load rates, total sediment load, mean diameter variation of bed material, and riverbed elevation changes for the years 2001, 2010, and 2022 due to land cover change. Further, it provides sediment erodibility and landslide index using rainfall-runoff-inundation model's simulations, remote sensing data and GIS to identify the potential landslide risk locations within the basin.

2. STUDY AREA AND DATA AVAILABILITY

2.1 Study area

The Kelani River Basin (Figure 1) is located between latitudes of 6° 47' and 7° 05' and longitudes of 79° 52' and 80° 13', spanning an area of 2,230 km² in the wet zone of Sri Lanka. The Kelani River is significant in Sri Lanka and flows towards the west coast of the country through Colombo, the Capital of the country. It supplies 80% of Colombo's drinking water needs and is used for hydropower generation in the upstream region. The basin experiences a mean annual rainfall of 3,718 mm, primarily due to the southwest monsoon. The terrain of the basin naturally divides it into two basins: the upper basin, which is characterized by steep terrain, and the lower basin, which is a floodplain (De Silva et al., 2012). The lower basin is prone to frequent flooding due to its orientation, topography, and

poor drainage (Dissanayaka and Rajapakse, 2019).

2.2 Data availability

The Moderate Resolution Imaging Spectrometer (MODIS) yearly global land cover product (MCD12Q1) with a spatial resolution of 500 m for 2001, 2010, 2016, 2018, and 2022 was downloaded from the USGS Earth Explorer website. The land-use maps were reclassified according to the International Geosphere-Biosphere Program (IGBP) global vegetation classification scheme (Sulla-Menashe and Friedl, 2018) for the years 2001, 2010, 2016, 2018, and 2022. In addition, these maps were verified based on the maps revised by the Survey Department, Sri Lanka.

Hydrological data and maps based on SHuttle Elevation Derivatives at multiple Scales (HydroSHEDS) 15-arc (~500 m) digital elevation model (DEM) were used for delineating topographic maps such as elevation, flow accumulation, and flow direction for the basin using the ArcGIS hydro tools.

FAO/ UNESCO soil map of the world at 1: 5 000 000 scale was used to classify the soil texture classification over the basin to define the soil properties shown in Figure 2. Soil properties according to soil texture classification are given in Table 1.

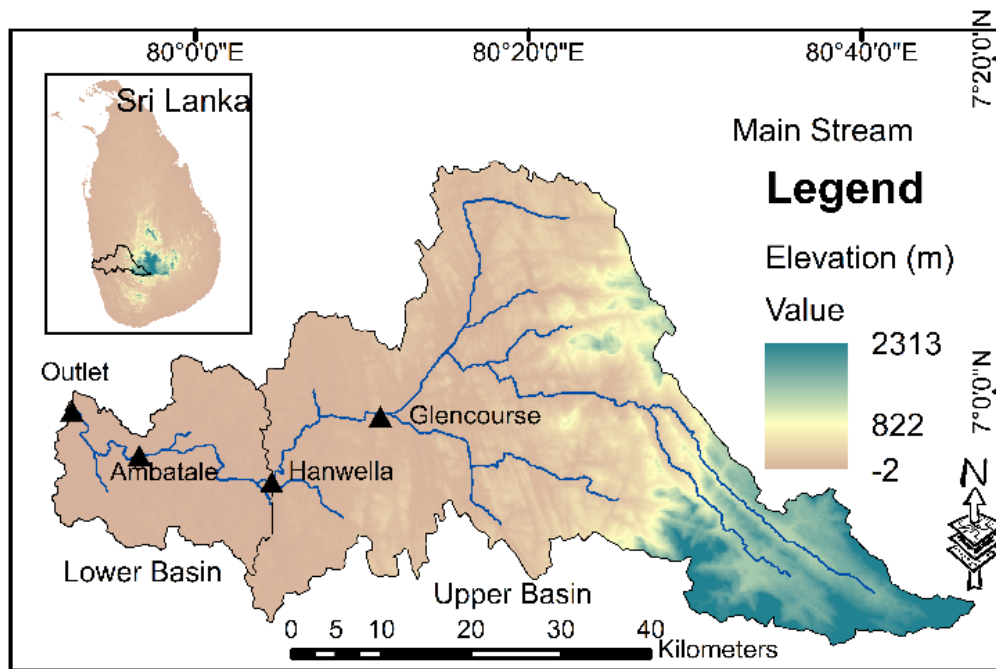


Figure 1: Study map (Kelani River Basin)

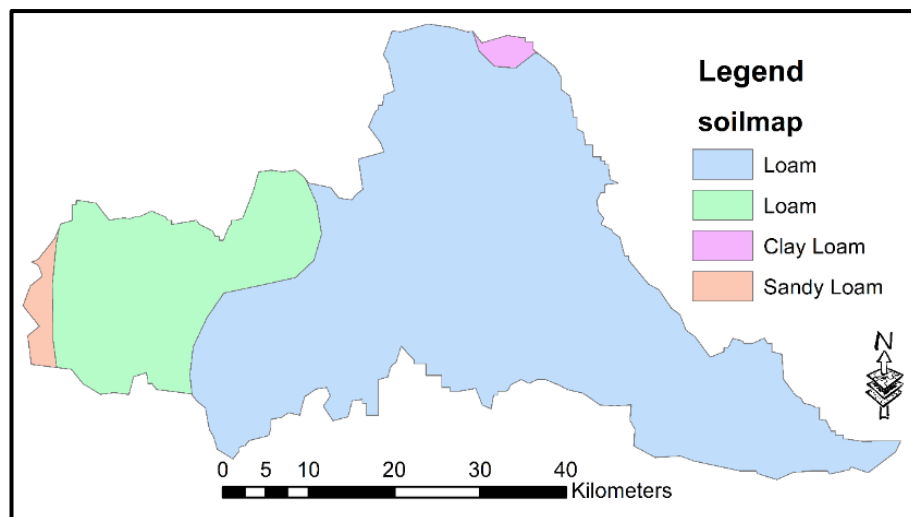


Figure 2: Soil map of the Kelani River Basin

Table 1: Porosity for each soil texture

Soil Texture	Loam	Clay Loam	Sandy Loam
Porosity	0.463	0.464	0.453

3. METHODOLOGY

3.1 Rainfall-Sediment-Runoff Model

The rainfall-sediment-runoff (RSR) model is an integration of a rainfall-runoff-inundation

(RRI) model and a sediment runoff model that provides flow discharge, bedload, and suspended load rates as outputs. The rainfall-runoff model deals with slopes and river channels, separately and calculates river flow using a 1D diffusion

wave equation and flow on slope grids using a 2D diffusion wave equation. The sediment model considers the river network as a series of unit channels, each defined as a channel section with two inflow points and one outflow point (Shinji et al., 2000). This model does not account for the sediment from the upstream ends of most upstream unit channels due to the rare occurrence of sediment supply as a form of bedload in the upstream slopes. The governing equations for the RSR model in unit channels are given by the following. The inflow points of the unit channel are represented by x_i and y_i , while the outflow point is represented by x_{i+1} .

The continuity equation for flow discharge is

$$\frac{\partial h_{i+1}}{\partial t} = \frac{1}{BL} [Q(x_i) + Q(y_i) - Q(x_{i+1}) + q_{i+1}L_{i+1}], \quad (1)$$

where, h_{i+1} , B , and L are the surface water depth, flow width, and length of the unit channel; t is time, $Q = (1/n)t^{1/2}h^{5/3}B$ where Q , n , i , h , and B are flow discharge, Manning's roughness, bed slope, surface water depth, and flow width, respectively. $Q(x_i)$, $Q(y_i)$ and $Q(x_{i+1})$ are the discharges of the unit channel at inflow points x_i and y_i and outflow point x_{i+1} , respectively.

The convection equation for sediments in suspension is

$$\frac{\partial hc_j}{\partial t} = \frac{1}{(BL)} \{c_{sj}(x_i)Q(x_i) + c_{sj}(y_i)Q(y_i) - c_{sj}(x_{i+1})Q(x_{i+1})\} - D_{sj}(x_{i+1}) + E_{sj}(x_{i+1}), \quad (2)$$

where, c_j , $c_{sj}(x_i)$, $c_{sj}(y_i)$ and $c_{sj}(x_{i+1})$ are the suspended sediment concentration, sediment concentration of the unit channel for sediment size class j at inflow points x_i and y_i and

outflow point x_{i+1} , respectively. $D_{sj}(x_{i+1})$ and $E_{sj}(x_{i+1})$ are the deposition and erosion rates of the suspended sediment for the sediment size class j . The deposition and erosion rates are given by Harada et al.'s formulae (2019). $E_{sj} = W_e f_{bj} c_s$ and $D_{sj} = w_{oj} c_j$, where W_e , f_{bj} , c_s , w_{oj} , and c_j are the entrainment velocity, sediment fraction, sediment concentration of the bedload layer, settling velocity, and suspended sediment concentration for sediment size class j , respectively.

The sediment continuity equation is

$$\frac{\partial z}{\partial t} = \frac{1}{(1-\lambda)} \sum_j \left[\frac{1}{BL} \{Q_{bj}(x_i) + Q_{bj}(y_i) - Q_{bj}(x_{i+1})\} + D_{sj}(x_{i+1}) - E_{sj}(x_{i+1}) \right] \quad (3)$$

where z is the riverbed elevation; λ is the porosity of bed sediment; $Q_{bj}(x_i)$, $Q_{bj}(y_i)$, and $Q_{bj}(x_{i+1})$ are the bedload rates of the unit channel for the sediment size class j at inflow points x_i and y_i and outflow point x_{i+1} , respectively. Bedload rates are given by Egashira et al.'s formulae (1997, 2005) as $q_{b*j} =$

$4.4 p_j \tau_{*j}^{5/2}$ which is similar to

$q_{bj}/\sqrt{(s-1)gd^3}$, where q_{b*} , s , d , and τ_{*j} are the non-dimensional bedload rate per unit time and unit length, the relative density of the sediment particles, sediment size, and non-dimensional bed shear stress respectively. The factor of 4.4 is an estimated parameter following the original formulae.

The temporal change of sediment grain size fraction for the first layer of each unit channel is

$$\frac{\partial P_j}{\partial t} = \frac{1}{(1-\lambda)\delta BL} \{Q_{bj}(x_i) + Q_{bj}(y_i) -$$

$$Q_{bj}(x_{i+1})\} + D_{sj}(x_{i+1}) - E_{sj}(x_{i+1}) - \frac{\partial z f_j}{\partial t \delta} \quad (4)$$

where $\sum_1^N p_j = 1$,

$$f_j = \begin{cases} p_{j2} & \text{when } \frac{\partial z}{\partial t} \leq 0 \\ p_j & \text{when } \frac{\partial z}{\partial t} > 0 \end{cases}, \quad p_j \text{ is the fraction of}$$

sediment size class j ; δ is the depth of the surface layer; p_{j2} is the fraction of sediment size class j in the second layer underneath the exchange layer.

3.2 Sediment erodibility/landslide index

The RSR model considers two types of sediment transport; bedload and suspended load. These two types are primarily controlled by flow discharge. Another type of sediment transport is landslide debris flow which is not included in the RSR model of the present study due to time constraints and data limitations. Landslide debris flow differs significantly from the bedload and suspended load, as it is influenced by the subsurface flow and stability of soil layers. Changes in land cover can lead to an increase or decrease in landslide hazards (Chen et al., 2019), with numerous landslides directly delivering sediment to rivers and significantly altering the sediment stored volume in river channels (Broothaerts et al., 2012). Therefore, it is important to conduct a sensitive analysis of landslides in the basin focusing on sediment erodibility, and landslide index.

The sediment erodibility of a surface area is dependent on the bed shear stress, which can be represented as $\tau = \rho g h i$, where h is the surface water depth, i is the bed slope, ρ is the water density, and g is the gravitational acceleration. In this context, ρ and g remain constant. Thus,

sediment erodibility can be expressed as:

$$\text{Sediment erodibility} = h i. \quad (5)$$

The landslide index is influenced by subsurface flow, and thus, it can be defined as:

$$\text{Landslide Index} = h_s i / d, \quad (6)$$

where h_s is the subsurface water depth, and d is the soil depth.

4. SIMULATION CONDITIONS

4.1 RSR model

RSR model calibration and validation were carried out for the flood events in 2016 and 2018, respectively, for both the rainfall-runoff model and sediment model using the observed hourly discharge data at Glencourse and measured hourly sediment concentration at the Ambatale water treatment plant. Here, sediment concentration data were determined based on the turbidity measurements at the Ambatale water treatment plant using the portable turbidity meter HACH 2100 P. The results of calibration and validation of the rainfall-runoff model are given in Figure 3. The rainfall-runoff model performed well for the 2016 and 2018 floods with the Nash-Sutcliffe coefficient of 0.8 and 0.7, respectively.

Accordingly, the calibrated parameter values are 0.04, 1 m, and 0.085 m/s for Manning's roughness of the river channel, soil depth, and lateral saturated hydraulic conductivity respectively. Here, we defined the effective Equivalent roughness of slopes (n_s) based on the land use type, and soil porosity (p) based on soil texture through the literature (Pakoksung 2016) as given in Table 2.

The results of calibration and validation of the sediment model are given in Figure 4. The initial

sediment grain size distribution in Table 3 was defined by calibrating the model and considering field data measured during January 2023.

To investigate the impacts of the land use on rainfall-runoff and sediment transport processes

for 2001, 2010, and 2022, the simulations of the RSR model were carried out using the 2016 flood (10-year flood) data using corresponding land use maps of the year for 2001, 2010, and 2022. The parameters were defined according to the land use types given in Table 2.

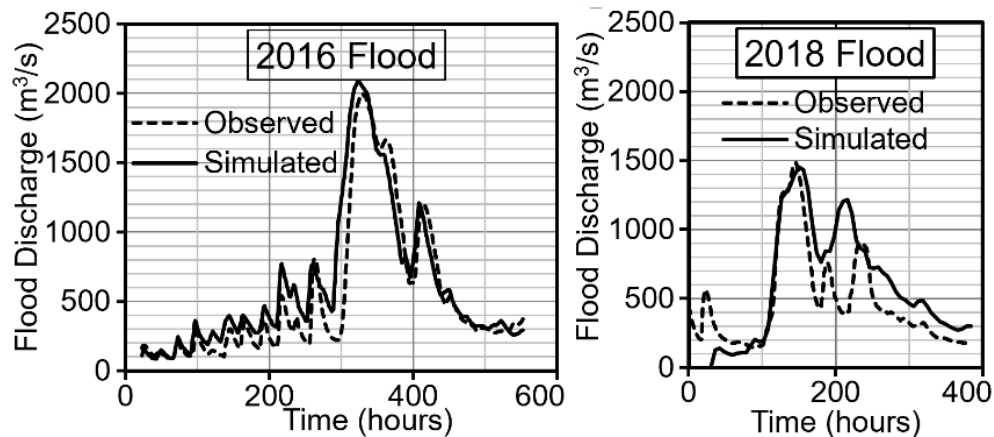


Figure 3: Rainfall-runoff model calibration and validation

Table 2: Manning's roughness and soil porosity of each land use type

Land use	Forest	Woody savannas	Grassland	Wetland	Cropland	Urban	Water bodies
n_s	0.85	0.45	0.3	0.5	0.3	0.05	0.05
p	0.463	0.463	0.463	0.463	0.463	0.001	0.463

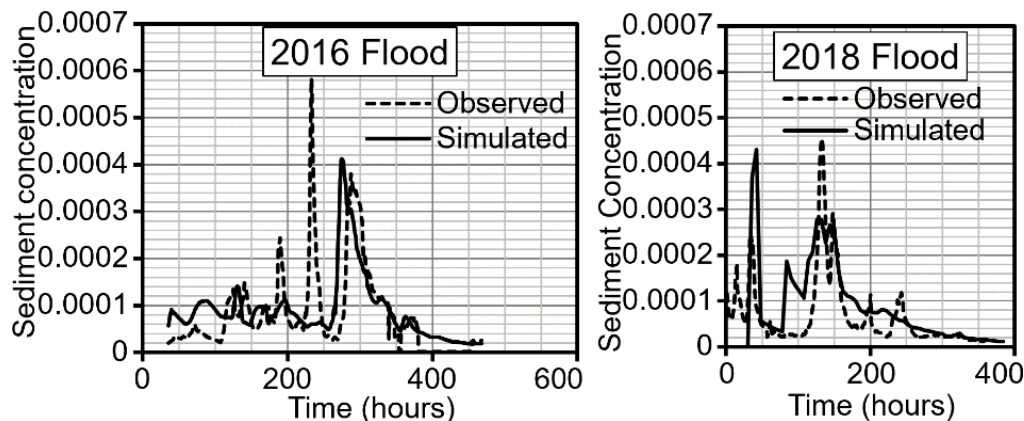


Figure 4: Sediment model calibration and validation

Table 3: Initial sediment grain size distribution

Sediment grain size (mm)	0.037	0.11	0.225	0.45	0.89	1.77	3.55	8.72	31.35	700	1200
Fraction %	0	0	1	3	7	10	19	28	28	2	2

4.2 Sediment erodibility/landslide index

The Shuttle Radar Topography Mission (SRTM) 3-arc (90 m) DEM was utilized to determine sediment erodibility and the landslide index. Here, h and h_s are determined using the RRI model that was developed using the Shuttle Radar Topography Mission (SRTM) 3-arc (90 m) DEM.

The calibration results of the RRI model are presented in Figure 5, and the calibrated parameters are 0.04, 0.85, 2m, 0.025 m/s, and 1500 for Manning's roughness for the river channel, equivalent roughness for slope cells, soil depth, saturated hydraulic conductivity, and threshold, respectively. Figure 6 depicts the values of h , h_s and slope (i) over the basin for the 2016 flood (10-year flood).

5. RESULTS AND DISCUSSION

5.1 Land-use change analysis

Figure 7 shows the MODIS land cover map for the years 2001, 2010, and 2022 prepared according to the IGBP classifications. According to Figure 7, the Kelani River Basin comprises four major land use types, namely Forest, Cropland, Woody Savannas, and Urban areas.

The upper basin is predominantly covered by woody savannas and forest areas, while downstream areas are dominated by cropland and urban areas.

Accordingly, the area percentage of the major land use types in the Kelani River basin for 2001, 2010, and 2022 are illustrated in Figure 8. In all years, 2001, 2010, and 2022, woody savannas account for the majority of the area, exceeding 48%. Forest areas were 33% in 2001 but depleted to around 20% by 2010 and 2022. Cropland and urban areas constituted approximately 13% and 7% of the area, respectively.

Figure 9 displays the changes in the area percentage of the major land use types in 2010 and 2022, compared to the year 2001. Urban areas and woody savannas show an increasing trend, while cropland and forest areas exhibit a decreasing trend. In 2010, forest areas decreased by approximately 15%, while woody savannas increased by the same amount. By 2022, the forest area had increased by approximately 5% compared to 2010, while woody savannas had reduced by 7% compared to 2010. Urban areas increased by only 0.7% and 2% in 2010 and 2022, respectively, compared to 2001.

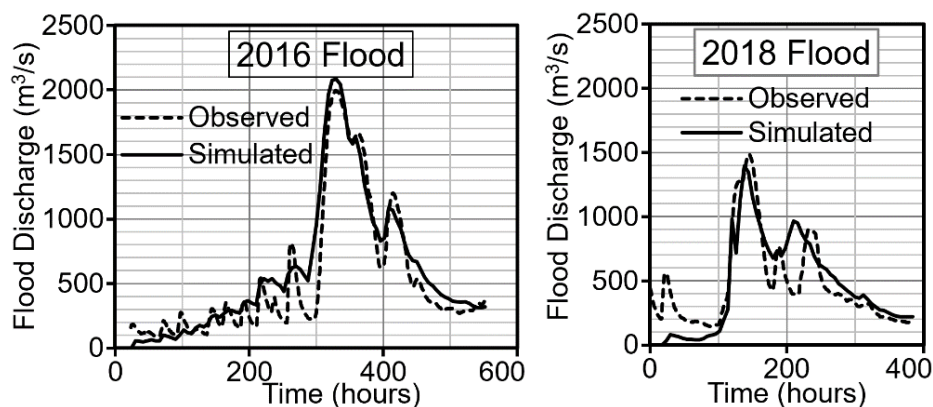


Figure 5: RRI model's calibration and validation results

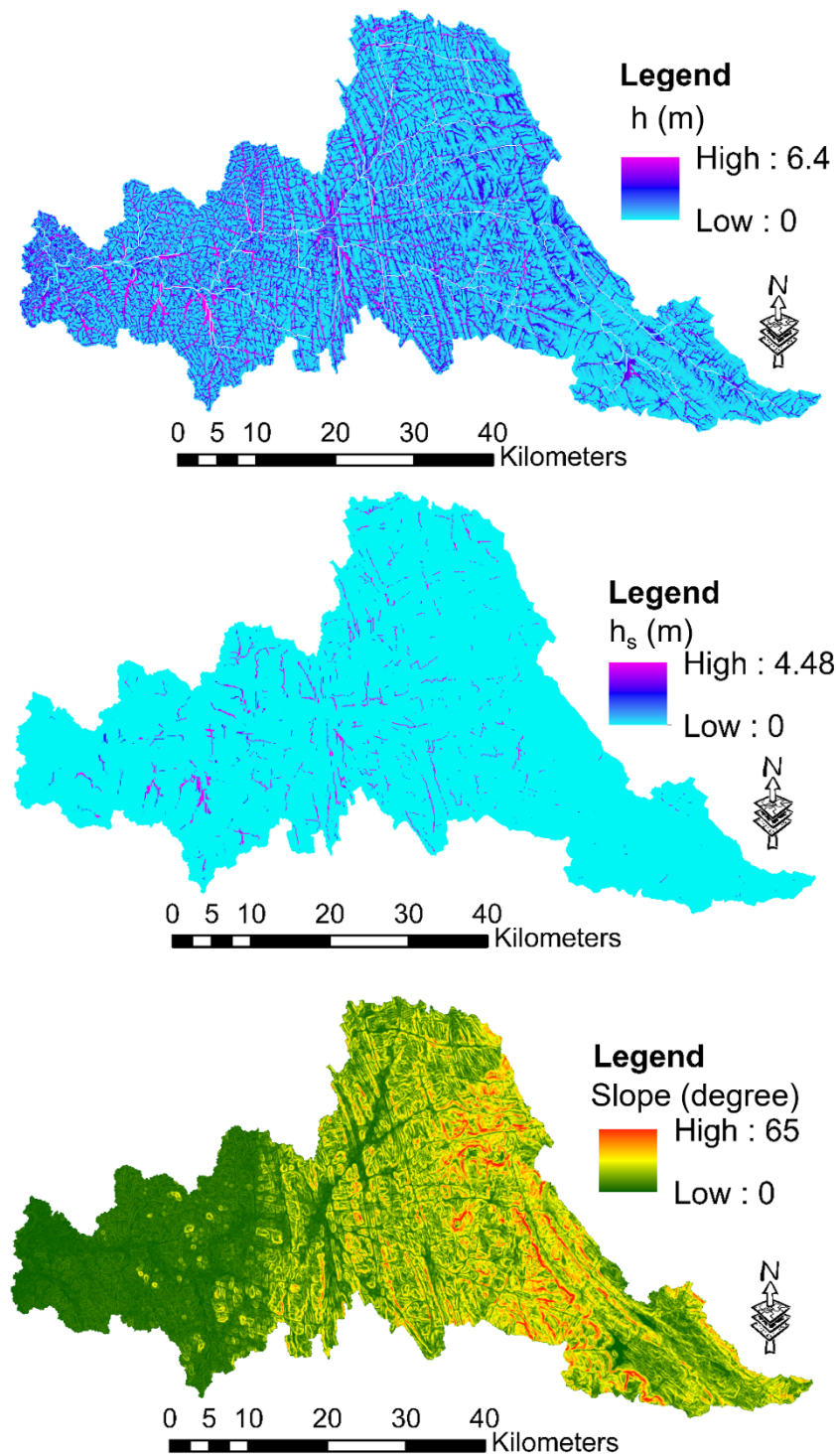


Figure 6: h , h_s , and slope for a 10-year flood

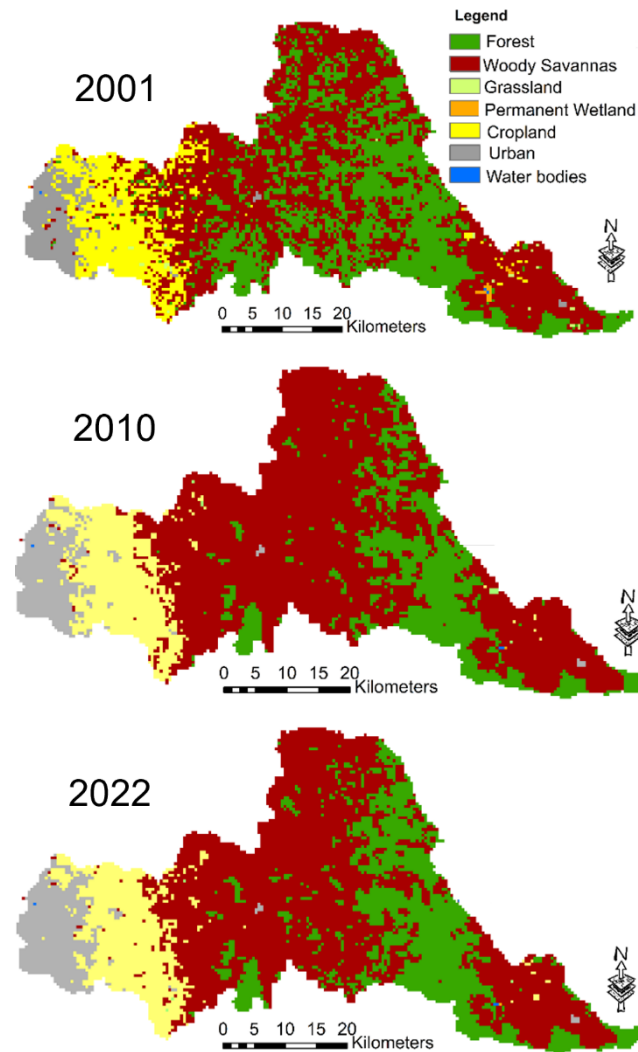


Figure 7: MODIS land cover maps for 2001, 2010, and 2022

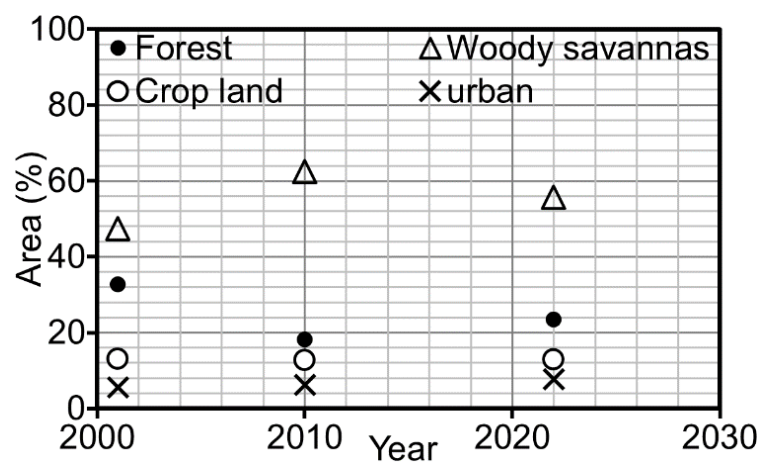


Figure 8: Total land use area (%) for 2001, 2010, and 2022

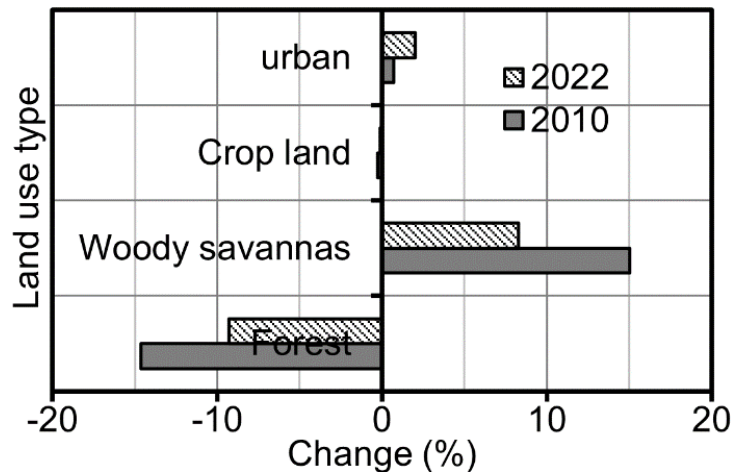


Figure 9: Land use change in (%) in 2010 and 2022 compared to 2001

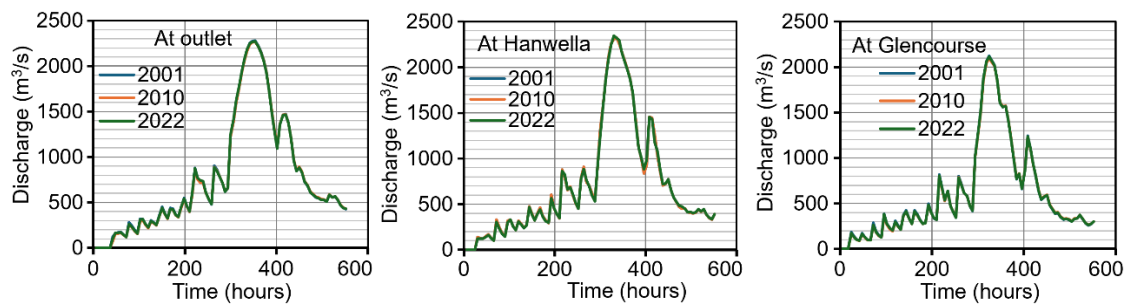


Figure 10: Flow runoff variation at each location for 2001, 2010, and 2022

Table 4: Peak flow discharge (m³/s) at each location for 2001, 2010, and 2022

Location	Outlet	Hanwella	Glencourse
2001	2,255	2,283	2,048
2010	2,264	2,306	2,069
2022	2,251	2,285	2,055

5.2 Runoff variation for 10-year flood

Figure 10 illustrates the variations in runoff for the 2016 flood (10-year flood) at outlet, Hanwella, and Glencourse in Figure 1 for the years 2001, 2010, and 2022. The data presented in Figure 10 shows that the runoff variation at outlet, Hanwella, and Glencourse for the years 2001, 2010, and 2022 is almost identical. Table 4 provides peak discharge values at each location for 2001, 2010, and 2022. As can be observed from Table 4, the peak discharge at all selected locations in 2010 is slightly higher than in 2001 and 2022 due to the depletion of the forest area in 2010 compared to

the years 2001 and 2022. The peak discharge at Hanwella and Glencourse in 2010 and 2022 is slightly higher than in 2001 due to the depletion of the forest area compared to the year 2001, where both locations' upstream land area is covered predominantly by forest and woody savannas. The peak discharge changing percentage at outlet, Hanwella, and Glencourse in 2010 compared to 2001 are about 0.4%, 1%, and 1%, respectively, while the peak discharge changing percentage at outlet, Hanwella, and Glencourse in 2022 compared to 2001 are about -0.14%, 0.1%, and 0.34%, respectively.

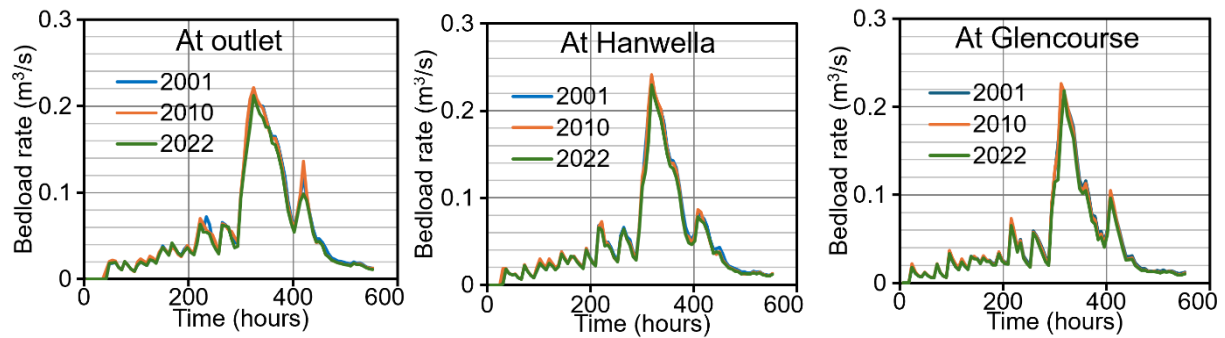


Figure 11: Bedload rate variation at outlet, Hanwella, Glencourse for 2001, 2010, and 2022

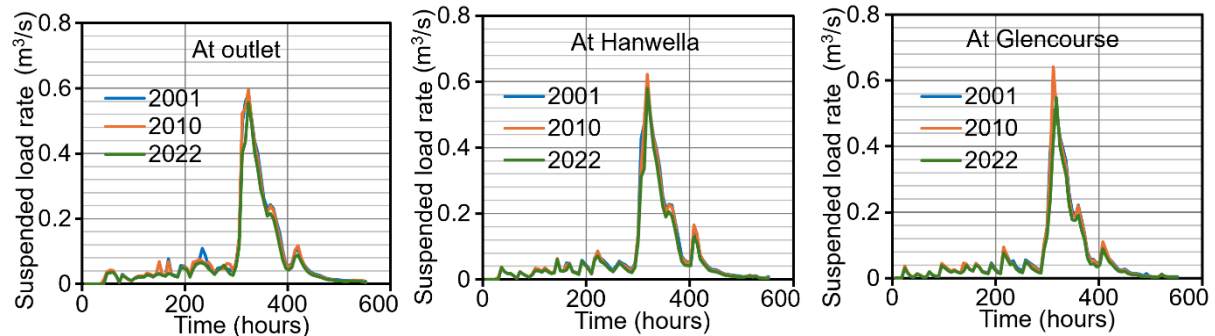


Figure 12: Suspended load rate at outlet, Hanwella, Glencourse for 2001, 2010, and 2022

Table 5: Peak bedload/ suspended load rates at Outlet, Hanwella, and Glencourse for 2001, 2010, and 2022

Year	Bedload rate (m ³ /s)			Suspended load rate (m ³ /s)		
	Outlet	Hanwella	Glencourse	Outlet	Hanwella	Glencourse
2001	0.2160	0.2338	0.2116	0.5828	0.6087	0.5117
2010	0.2213	0.2415	0.2265	0.5958	0.6225	0.6416
2022	0.2120	0.2298	0.2182	0.5554	0.5799	0.5473

5.3 Bedload rate and Suspended load rate variation for the 10-year flood

Figure 11 and 12 depict the variations in bedload and suspended load rates, respectively, at outlet, Hanwella, and Glencourse. The data presented in Figure 11 and 12 indicates that the variation of bedload and suspended load rates in 2010 is slightly higher at peaks compared to the years 2001 and 2022 due to the low forest area in 2010 compared to the years 2001 and 2022, which caused the high peak discharge in 2010 presented in Table 4. Table 5 provides the peak bedload and suspended load rates at outlet,

Hanwella, and Glencourse for 2001, 2010, and 2022. As can be observed from Table 5, the peak bedload and suspended load rates in 2010 are higher than in 2001 and 2022 due to the high peak discharge. The bedload and suspended load rates at outlet and Hanwella in 2022 were slightly lower than in 2001 and 2010, possibly due to variations in flow, sediment grain size, and riverbed elevations caused by land use changes. However, at Glencourse, the peak bedload and suspended load rates in 2010 and 2022 were higher than in 2001, likely due to the depletion of the forest area. The percentage changes in peak bedload rates in 2010 were 2.4%, 3.4%, and 7.0 %

at outlet, Hanwella, and Glencourse, respectively, while the changes in peak suspended load rates were 2.2%, 2.3%, and 25%, at outlet, Hanwella, and Glencourse, respectively. The variation in peak bedload and suspended load rates at Glencourse was higher than at outlet and Hanwella due to its greater sensitivity to changes in the upstream forest layer. The peak bedload and suspended load are more sensitive to changes in flow discharge caused by land cover alterations. According to Manning's formula employed in equation (1), flow depth is proportional to flow discharge raised to the power of $3/5$. The bed shear stress is proportional to flow discharge raised to the power of $3/5$. The bedload rate in equation (3) is proportional to bed shear stress raised to the power of $5/2$ and the bedload rate is proportional to flow discharge raised to the power

of $3/2$ $q_b \sim Q^{3/2}$. Therefore, bedload rate changes highly sensitive.

5.4 Total loads for the 10-year flood

Figure 13 shows the total load at the three locations in 2001, 2010, and 2022. The total load is calculated as the total area under both bedload and suspended load rate curves shown in Figures 11 and 12. The total load in 2022 was lower than in 2001 and 2010 at all three locations, with no significant difference between 2001 and 2010. These differences occurred due to variations in flow, riverbed, and sediment grain size. The decrease in suspended load in 2010 and 2022 was greater than the decrease in bedload, indicating that suspended load is more sensitive than bedload due to sediment transport being dominated by suspension in the Kelani River.

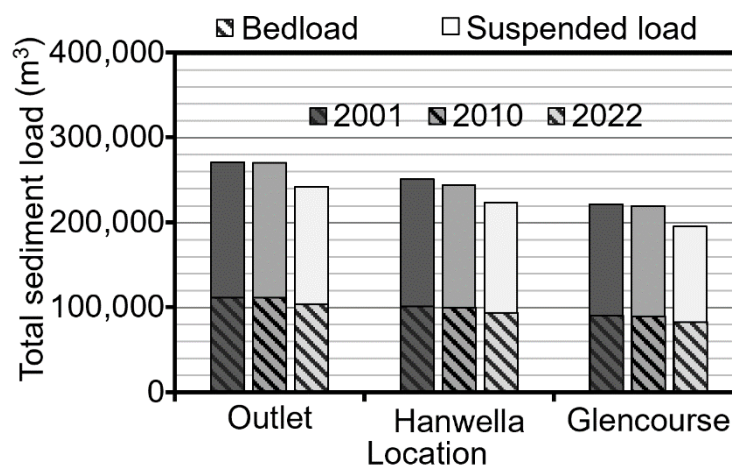


Figure 13: Total sediment load at outlet, Hanwella, and Glencourse for 2001, 2010, and 2022

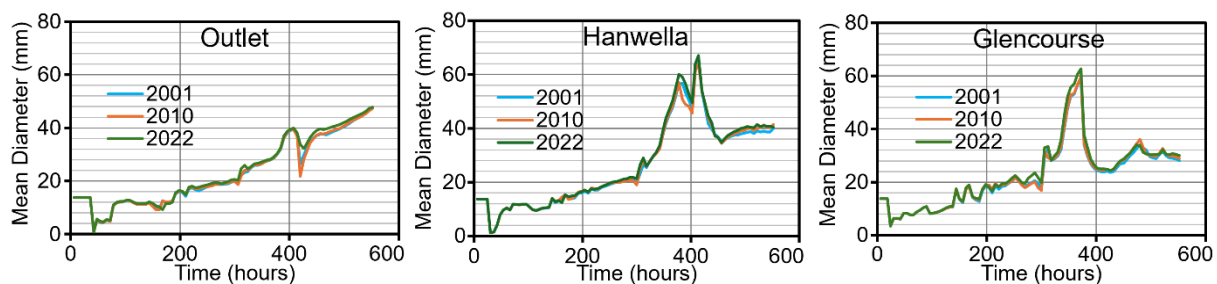


Figure 14: Mean diameter variation at outlet, Hanwella, and Glencourse for 2001, 2010, and 2022

5.5 Mean diameter variation of riverbed material for the 10-year flood

Figure 14 presents the average diameter fluctuation of riverbed material at the outlet, Hanwella, and Glencourse during the 10-year flood in 2001, 2010, and 2022. As illustrated in Figure 14, there is a slight variation in the mean diameter of bed material in 2001, 2010, and 2022. During the flood event, the riverbed material becomes coarser due to increased sediment transport capacity resulting from increased flow discharge. Following the flood, the riverbed material suddenly becomes finer with reduced discharge, eventually reaching a stable sediment condition in the riverbed.

5.6 Riverbed variation for 10-year flood

Figure 15 displays the overall riverbed elevation change in 2001, showing the difference in total riverbed elevation in 2010 and 2022 compared to 2001 for the 2016 flood (10-year flood). As shown in Figure 15, most of the downstream channels experience erosion of 0 to 0.5 m, while there is a trend of deposition in the upstream channels. The tendencies of erosion or deposition in the channels are influenced by factors such as river morphology, hydraulics, and hydrological conditions. The difference in deposition or erosion elevation of riverbeds in 2010 and 2022 compared to 2001 ranges from 0 to 9 cm due to land use changes, indicating that changes in riverbed elevation due to land use changes are substantial. These changes in riverbed elevation led to changes in sediment transport as well as water depths.

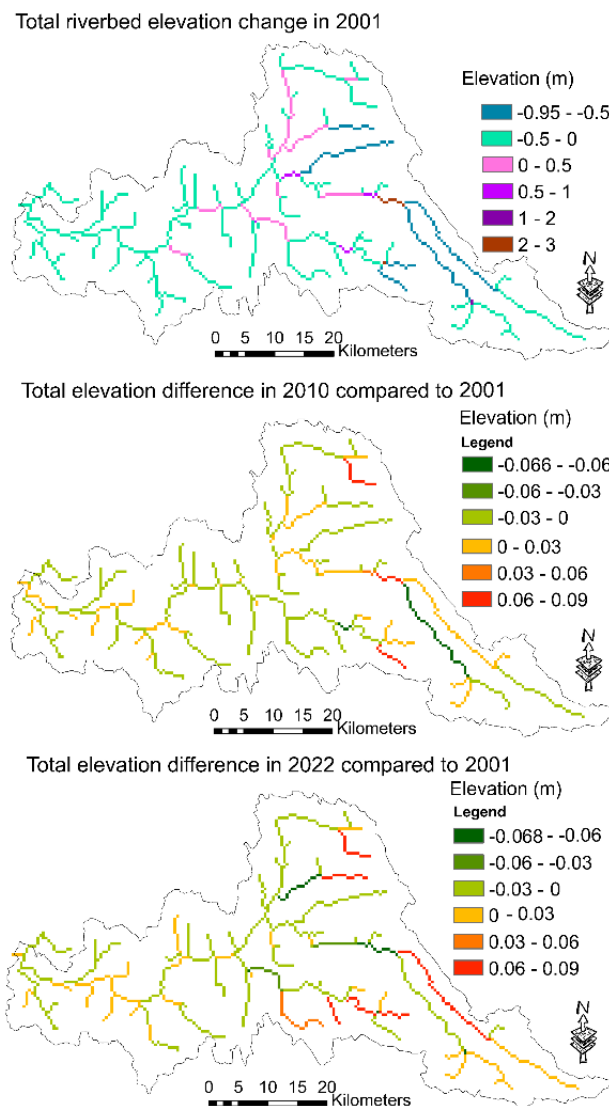


Figure 15: Total riverbed elevation changes in 2001 and the total riverbed elevation difference in 2010, and 2022 compared to 2001

5.7 Sediment erodibility/ landslide index

Figure 16 displays the erodibility and landslide index along with historical landslides from 2003 to 2022. The sediment erodibility and landslide index are higher in the middle of the Kelani River Basin, indicating that landslides are more likely to occur in that region. According to the historical landslides from 2003 to 2022, landslides have occurred in areas where sediment erodibility and landslide index are high. Furthermore, the high

landslide index observed in the downstream region can be noted, despite the terrain being flat and the slope size insignificant in Figure 6.

Consequently, although the landslide index is elevated, the likelihood of landslide occurrence remains minimal.

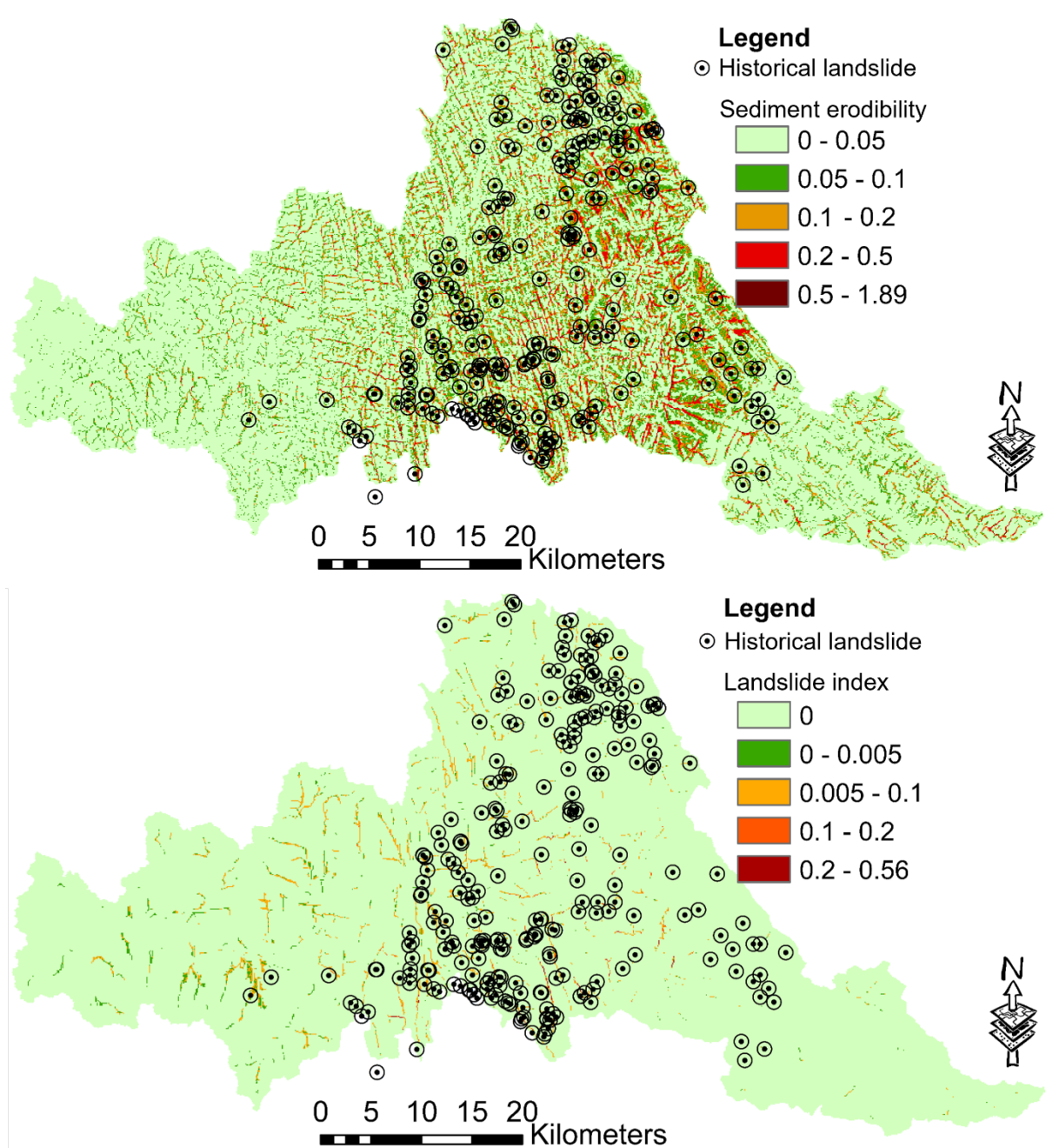


Figure 16: Erodibility and landslide index with historical landslide from 2003 to 2022

6. CONCLUSIONS

In this study, we evaluated the effects of land use change on rainfall-runoff and sediment transport processes in the Kelani River, where the river environment is increasingly degraded by

anthropogenic activities particularly urbanization and sand mining activities. The evaluation was based on the analysis of land cover maps, evaluation of flood hydrographs, bedload rates, suspended load rates, total sediment load, mean diameter variation of bed material, bed elevation

change, and soil erosion/ landslide indices using the rainfall-sediment-runoff model, remote sensing data, and GIS. The conclusions of this study are as follows.

1. There has been an increasing trend in woody savanna and urban areas, while forest and cropland areas have experienced a decline in both 2010 and 2022 compared to 2001. Among the main land use types in the basin, which include woody savannas, forest, cropland, and urban areas, changes in woody savannas and forest in 2010 and 2022 compared to 2001 are particularly notable.
2. This study emphasizes that the sediment transport processes in the basin are more susceptible to change than the rainfall-runoff processes affected by land cover changes. The total sediment loads for both 2010 and 2022 exhibit a downward trend, with a more pronounced decrease in 2022 compared to 2001. This decrease can be attributed to changes in land use, resulting in a reduction of approximately 10%. The alteration in riverbed elevation due to land use changes is significant, varying between 0 and 9 cm compared to 2001.
3. The middle region of the basin is particularly vulnerable to landslides and soil erodibility, as evidenced by higher erodibility and landslide index values in this area. The vulnerability highlights the urgent need for land use management strategies aimed at mitigating erosion risks.

ACKNOWLEDGEMENT

The Authors wish to thank the International

Centre for Water Hazard and Risk Management (ICHARM) for the RSR model access, the Irrigation Department, the Meteorology Department, the National Water Supply and Drainage Board, the National Building Research Organization of Sri Lanka for the meteorological, hydrological, and landslide data, the National Aeronautics and Space Administration (NASA), United States Geological Survey (USGS), World Wildlife Fund (WWF), and Food and Agriculture Organization of the United Nations (FAO) for open access satellite data, and the Department of Civil Engineering of the University of Moratuwa for the laboratory facilities, and Dr. Toru Konishi, and Prof. Hideo Amaguchi for feedback.

FUNDING STATEMENT

This research was supported by the Tokyo Metropolitan Government Advanced Research Grant Number (R4-2).

REFERENCES

- Abeshu, G. W., H. Y. Li, Z. Zhu, Z. Tan, L. R. Leung, and H. Y. Li. 2022. "Median Bed-Material Sediment Particle Size across Rivers in the Contiguous US." *Earth System Science Data*, 14 (2). Copernicus Publications: 929–42. doi:10.5194/ESSD-14-929-2022.
- Areu-Rangel, O. S., M. Á. Hernández-Hernández, and R. Bonasia. 2024. "Land-Use-Change-Driven Erosion and Sediment Transport in the Yaqui River Sub-Basin (Mexico): Insights from Satellite Imagery and Hydraulic Simulations." *Land*, 13(11), 1846. doi:10.3390/LAND13111846.
- Broothaerts, N., E. Kissi, J. Poesen, A. Van Rompaey, K. Getahun, E. Van Ranst, and J. Diels. 2012. "Spatial Patterns, Causes and

- Consequences of Landslides in the Gilgel Gibe Catchment, SW Ethiopia.” *CATENA*, 97, 127–36. doi:10.1016/J.CATENA.2012.05.011.
- Chen, L., Z. Guo, K. Yin, D. P. Shrestha, and S. Jin. 2019. “The Influence of Land Use and Land Cover Change on Landslide Susceptibility: A Case Study in Zhushan Town, Xuan’en County (Hubei, China).” *Natural Hazards and Earth System Sciences*, 19 (10), 2207–28. doi:10.5194/NHESS-19-2207-2019.
- Chirachawala, C., S. Shrestha, M. S. Babel, S. G.P. Virdis, and S. Wichakul. 2020. “Evaluation of Global Land Use/Land Cover Products for Hydrologic Simulation in the Upper Yom River Basin, Thailand.” *Science of The Total Environment*, 708, 135148. doi:10.1016/J.SCITOTENV.2019.135148.
- Choi, W., and B. M. Deal. 2008. “Assessing Hydrological Impact of Potential Land Use Change through Hydrological and Land Use Change Modeling for the Kishwaukee River Basin (USA).” *Journal of Environmental Management*, 88 (4), 1119–30. doi:10.1016/J.JENVMAN.2007.06.001.
- Choto, M., and A. Fetene. 2019. “Impacts of Land Use/Land Cover Change on Stream Flow and Sediment Yield of Gojeb Watershed, Omo-Gibe Basin, Ethiopia.” *Remote Sensing Applications: Society and Environment*, 14, 84–99. doi:10.1016/J.RSASE.2019.01.003.
- CRIP. 2018. “Climate Resilience Improvement Project; Strategic Environmental Assessment of Development of River Basin Level Flood and Drought Mitigation Investment Plans (DBIP).”
- Daramola, J., E. J. Adepehin, T. M. Ekhwan, L. K. Choy, J. Mokhtar, and T. S. Tabiti. 2022. “Impacts of Land-Use Change, Associated Land-Use Area and Runoff on Watershed Sediment Yield: Implications from the Kaduna Watershed.” *Water*, 14(3), 325. doi:10.3390/W14030325.
- Dissanayaka, K. D.C.R., and R. L.H.L. Rajapakse. 2019. “Long-Term Precipitation Trends and Climate Extremes in the Kelani River Basin, Sri Lanka, and Their Impact on Streamflow Variability under Climate Change.” *Paddy and Water Environment*, 17 (2), 281–89. doi:10.1007/S10333-019-00721-6/TABLES/5.
- Egashira, S., and T. Itoh. 2006. “Paradoxical Discussions on Sediment Transport Formulas.” *River, Coastal and Estuarine Morphodynamics: RCEM 2005 - Proceedings of the 4th IAHR Symposium on River, Coastal and Estuarine Morphodynamics* 1: 33–38. https://jglobal.jst.go.jp/en/detail?JGLOBAL_ID=201902218923712199
- Egashira, S., and K. Matsuki. 2000. “A Method for Predicting Sediment Runoff Caused by Erosion of Stream Channel Bed.” *Proceedings of Hydraulic Engineering*, 44, 735–40. Japan Society of Civil Engineers. doi:10.2208/PROHE.44.735.
- Egashira, S., K. Miyamoto, and T. Ito. 1997. “Bed-Load Rate in View of Two Phase Flow Dynamics.” *Proceedings of Hydraulic Engineering*, 41, 789–794. Japan Society of Civil Engineers. doi:10.2208/PROHE.41.789.
- Güvel, Ş. P., 2024. “Assessment of the Impact of Land Cover Changes on Sediment Yield: A Case Study.” *Water Supply*, 24(3), 931–945. doi:10.2166/WS.2024.

- Harada, D., S. Egashira, T. S. Ahmad, and N. Katayama. 2019. "A Study on the Erosion Rate of Riverbeds Using the Entrainment Concept." *Journal of Japan Society of Civil Engineers Ser B1 ((Hydraulic Engineering)*, 75(2), I_967-I_972. 公益社団法人土木学会 doi:10.2208/JSCEJHE.75.2_I_967.
- Moisa, M. B., D. A. Negash, B. B. Merga, and D. O. Gemed. 2021. "Impact of Land-Use and Land-Cover Change on Soil Erosion Using the RUSLE Model and the Geographic Information System: A Case of Temeji Watershed, Western Ethiopia." *Journal of Water and Climate Change*, 12(7), 3404–20. doi:10.2166/WCC.2021.131.
- Ohana-Levi, N., A. Karnieli, R. Egozi, A. Givati, and A. Peeters. 2015. "Modeling the Effects of Land-Cover Change on Rainfall-Runoff Relationships in a Semiarid, Eastern Mediterranean Watershed." *Advances in Meteorology*, 2015(1), 838070. doi:10.1155/2015/838070.
- Pakoksung, K. 2016. "Runoff Analysis Using Satellite Data for Regional Flood Assessment - Spatial and Time Series Bias Correction of Satellite Data". 高知工科大学 . <https://kutarr.kochi-tech.ac.jp/records/600>.
- Santos, F. M. dos, R. P. de Oliveira, and J. A. Di Lollo. 2020. "Effects of Land Use Changes on Streamflow and Sediment Yield in Atibaia River Basin—SP, Brazil." *Water*, 12(6), 1711. doi:10.3390/W12061711.
- Silva, M. M. G. T. De, S. B. Weerakoon, S. Herath, U. R. Ratnayake, and S. Mahanama. 2012. "Flood Inundation Mapping along the Lower Reach of Kelani River Basin under the Impact of Climate Change." *Engineer: Journal of the Institution of Engineers, Sri Lanka* 45(2), 23. doi:10.4038/ENGINEER.V45I2.6938.
- Sourn, T., S. Pok, P. Chou, N. Nut, D. Theng, and P. V. V. Prasad. 2022. "Assessment of Land Use and Land Cover Changes on Soil Erosion Using Remote Sensing, GIS and RUSLE Model: A Case Study of Battambang Province, Cambodia." *Sustainability*. 14(7), 4066. doi:10.3390/SU14074066.
- Sulla-Menashe, D., and M. A. Friedl. 2018. "User Guide to Collection 6 MODIS Land Cover (MCD12Q1 and MCD12C1) Product." <https://lpdaac.usgs.gov/products/mcd12q1v006/>
- Zuo, D., Z. Xu, W. Yao, S. Jin, P. Xiao, and D. Ran. 2016. "Assessing the Effects of Changes in Land Use and Climate on Runoff and Sediment Yields from a Watershed in the Loess Plateau of China." *Science of The Total Environment*, 544, 238–50. doi:10.1016/J.SCITOTENV.2015.11.060